applied sciences

MDPI

Article

Ferrite-Loaded Inverted Microstrip Line-Based Artificial Magnetic Conductor for the Magnetic Shielding Applications of a Wireless Power Transfer System

Sonapreetha Mohan Radha [1], Seong Hoon Choi [1], Jae Ho Lee [2], Jung Hoon Oh [3], In-Kui Cho [3] and Ick-Jae Yoon [1,*]

[1] Department of Electrical Engineering, Chungnam National University, Daejeon 34134, Republic of Korea; sonapreetha@cnu.ac.kr (S.M.R.); choish413@o.cnu.ac.kr (S.H.C.)
[2] Department of Electronic Engineering, Kunsan National University, Gunsan 54150, Republic of Korea; jh_lee@ksnu.ac.kr
[3] Electronics and Telecommunications Research Institute (ETRI), Daejeon 34129, Republic of Korea; jhoh70@etri.re.kr (J.H.O.); cho303@etri.re.kr (I.-K.C.)
* Correspondence: ijyoon@cnu.ac.kr; Tel.: +82-42-821-5658

Abstract: In this paper, we propose a ferrite-loaded inverted microstrip line (IML)-based artificial magnetic conductor (AMC) with a novel design that can provide complete magnetic shielding at the backside of the transmitting (Tx) coil while slightly improving the power transfer efficiency (PTE) of a wireless power transfer system (WPTS). The target frequency of the WPTS application is approximately 6.78 MHz. In the proposed design, the AMC is placed behind the Tx coil, and its magnetic shielding capability and PTE performance were verified through simulations and measurements. The size of the proposed AMC is 528 × 528 × 6.6 mm^3. The measurement results verified that, compared with the Tx coil without an AMC surface, the proposed ferrite-loaded IML-based AMC can provide complete magnetic shielding while improving the PTE of the WPTS by approximately 8.05%.

Keywords: artificial magnetic conductor; high impedance surface; inverted microstrip line; magnetic shielding; magnetic field leakage reduction; metamaterial; reactive impedance surface; wireless power transfer system

check for updates

Citation: Radha, S.M.; Choi, S.H.; Lee, J.H.; Oh, J.H.; Cho, I.-K.; Yoon, I.-J. Ferrite-Loaded Inverted Microstrip Line-Based Artificial Magnetic Conductor for the Magnetic Shielding Applications of a Wireless Power Transfer System. *Appl. Sci.* **2023**, *13*, 10523. https://doi.org/10.3390/app131810523

Academic Editor: Evangelos Hristoforou

Received: 6 September 2023
Revised: 17 September 2023
Accepted: 20 September 2023
Published: 21 September 2023

Copyright: © 2023 by the authors. Licensee MDPI, Basel, Switzerland. This article is an open access article distributed under the terms and conditions of the Creative Commons Attribution (CC BY) license (https://creativecommons.org/licenses/by/4.0/).

1. Introduction

Recently, wireless power transfer systems (WPTSs) have gained more attention in various applications owing to their advantages of convenience and safe user experience. On the basis of their required operating distance and amount of power, they can be classified into radiative and non-radiative types [1–8]. A radiative WPTS is based on a range of microwave frequencies and laser techniques and is widely used in high-power and far-field applications. On the other hand, a non-radiative WPTS uses near-field coupling of electric or magnetic fields [6–8]. It is quite popular for short-distance applications such as charging consumer electronics, electric vehicles, and intra-vehicles. However, after a certain charging distance, its power transfer efficiency (PTE) decreases, and magnetic field leakage occurs. As shown in Figure 1, a stand-alone transmitting (Tx) coil can simultaneously generate a uniform magnetic field at its front and back. For charging applications, the receiving (Rx) coil is placed at the target area, and the magnetic field in the non-target area is called the magnetic field leakage. The magnetic field leakage can be harmful to people in the vicinity and cause electromagnetic interference to nearby equipment. According to the guidelines of the International Commission on Non-Ionizing Radiation Protection (ICNIRP), the magnetic field leakage should be minimized to a safe level of 270 mG for humans [9].

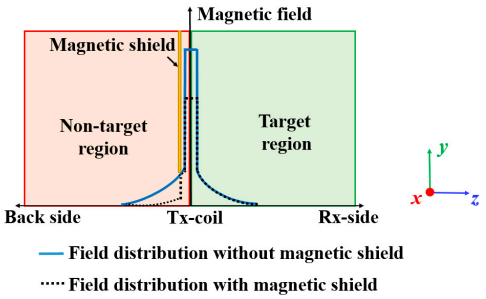


Figure 1. Representation of magnetic field leakage in a WPTS.

Several studies are underway to minimize magnetic field leakage and improve PTE [10–19]. For example, the PTE can be improved using coated wires such as litz and magneto-plated wires [10], by adding relay coils [11], or by using metamaterials [17–19]. For magnetic shielding, placement of ferromagnetic materials or ferrites behind the Tx and Rx coils are widely used in very low frequency (VLF) to low frequency (LF) applications [12], [13]. In previous studies [14–16], magnetic shielding has been implemented using additional active or passive cancelation coils placed behind the Tx coils, which can generate the magnetic field in the opposite direction to the backside of the Tx coil. Even though this work can greatly mitigate magnetic field leakage, the complexity of the system increases, and it is not quite useful enough to improve the PTE performance of WPTSs. Another approach for achieving complete magnetic shielding while improving the PTE is to use a perfect magnetic conductor (PMC) as a back plate, which can be realized by designing artificial magnetic conductors (AMCs) [20]. Ideally, the AMC can provide a $\pm 180^{\circ}$ reflection phase owing to its high surface impedance and parallel image current, and eliminate backward radiation while enhancing the radiation toward the front when it is placed behind the antenna [21–24]. As it acts as a reflector, greatly enhancing unidirectional radiation with increased efficiency, the AMC design is widely used in the microwave frequency of the low-profile, relatively high-gain antenna design. However, its use at a relatively low frequency is limited [24] because the size of the AMC depends on its wavelength, making it large at low-frequency applications.

Only a few studies have focused on using AMCs for WPTS applications. Wu et al. [25] performed a simulation using the ideal PMC condition and verified that it improved the PTE performance compared with using an ideal PEC behind the Tx coil. Shi et al. [26] designed an AMC for an operating frequency of 23 MHz. Meanwhile, Lawson et al. [27] designed an AMC using a ferrite substrate where the metallic frequency selective surface (FSS) pattern is placed directly on the ferrite to generate a frequency of 6.78 MHz, although the performance was verified only by simulations. The merit of these AMCs is in their magnetic shielding performances. However, the size of the former AMC is relatively large [26], and it is challenging to realize the FSS layer on the ferrite substrate in the latter AMC because it may cause manufacturing intolerance and losses [27]. In addition, the fabrication of the hole on the ferrite surface is complex and expensive, as commercially available ferrites with holes are not common.

In this paper, we propose a compact and thin ferrite-loaded AMC structure with a novel design for complete magnetic shielding and PTE improvement of WPTSs, which was obtained by utilizing an inverted microstrip line (IML) design. Furthermore, the additional manufacturing cost of the via hole for the AMC can be eliminated with proper placement selection of the ferrite tiles. The performance of the proposed design of the IML-based AMC was verified with a WPTS, which showed very good performance in terms of magnetic shielding while improving the PTE. The overall profile, weight, and complexity of the IML-based AMC structure were greatly improved compared with those of AMC-based magnetic shielding structures. The possible applications of the proposed AMC in the WPTS may include smart home appliances utilizing wireless charging features and wireless

charging stations for mobile devices in public areas, as well as wireless electric vehicle charging stations, where the electromagnetic exposure should be regulated.

2. Design of Ferrite-Loaded AMC

2.1. Concept of the AMC Design

An AMC is a type of periodic array structure with properties resembling those of PMCs. It consists of a ground plane and periodic metal patches, usually referred to as FSSs. Each patch can be connected to the ground with either via pins, as shown in Figure 2a, or via-less. The operating frequency and reflection characteristics of an AMC can be obtained by controlling the geometrical parameters, such as the height and shape of the metal patches or the spacing between them, or the material properties. In general, an AMC can be characterized by a parallel inductor and capacitor (*LC*) resonator, as shown in Figure 2b. In the LC circuit, the gap between the metal patches can generate the capacitance (C_P), and the inductance (L_p) can be generated from the current flow to the ground through the via from the metal patch layer.



Figure 2. Equivalent circuit of an LC resonator. (**a**) Conceptual description. (**b**) Equivalent circuit.

The operating frequency (f_c) and surface impedance (Z_S) of the AMC are determined from Equations (1) and (2) [19].

$$f_c = \frac{1}{2\pi\sqrt{L_P C_P}} \tag{1}$$

$$Z_S = \frac{j\omega L_P}{1 - \omega^2 L_P C_P} \tag{2}$$

From Equation (1), the resonant frequency can be reduced by increasing the L_p and C_p. Equation (2) indicates that the surface impedance of the parallel resonant circuit is directly proportional to L_p and inversely proportional to C_P. The surface impedance of the parallel resonant circuit decreases when the C_P increases. Thus, in general, the miniaturization of the AMC is based on the values of L_p and C_P. The value of L_p is usually controlled by the dimension of the patch and height of the substrate, while the capacitance is controlled by the fringing field that occurs at the gap between the metal patches. In general, the additional lumped capacitors are connected between the patch elements as a means of shifting down the operating frequency. There is usually a trade-off between the choice of L_p and C_P in terms of bandwidth and unit cell size. However, if the parameters such as the substrate height, dielectric constant, and effective length of the patch are kept constant, only by increasing the capacitance will the frequency be lowered with the reduced impedance and bandwidth. Therefore, it would be challenging, or even impossible, to design a dielectric substrate-only-based AMC compact for the target applications of 6.78 MHz using lumped capacitance, despite its simpler configuration and lower manufacturing cost.

2.2. Ferrite-Loaded AMC Unit Cell Design

To design a compact unit cell for the target frequency of 6.78 MHz, the inductance, along with the lumped capacitance, must be increased. Hence, the ferrite layer can be loaded between the ground plane and the metal patch layers. However, practical issues must be considered before creating the design. First, the choices of commercially available ferrite cores for the MHz frequency range are limited. Second, ferrites with a hole are not

commonly available, and punching a hole requires additional cost. Moreover, the use of a via pin is inevitable to increase the inductance for unit cell miniaturization. Thus, the right choice of ferrite tiles in terms of material properties and shape is important. In view of the manufacturing difficulties, the rounded square ferrite MP1040-200 from Laird was chosen. The permeability of the ferrite is approximately 310 at 7 MHz, and further details of the ferrite core can be found in [28]. Even though it is not strongly relevant to this work, it is worth noting that the biased ferrite is an anisotropic medium and its electromagnetic response will not be the same for the TE or TM incidences, and such characteristic could be encountered for more degrees of freedom in designing AMC structures [29].

The configuration of the proposed unit cell is shown in Figure 3. The unit cell is composed of four subunit cells at the top, the ground at the bottom, and the ferrite core stacked on it, as shown in Figure 3a,b. An air gap is present between the ferrite core and the patch layer and can be either a suspended microstrip line (SML) type (Figure 3c) or an IML type (Figure 3d) depending on the relative position of the dielectric substrate to the metal patches. In both types, a via pin is connected between the ground plane and the metal layer. The unit cell length and width p are fixed as 105.6 mm, considering the available ferrite size. A single rounded square ferrite has a size of 26.4 (l_f) × 26.4 (w_f) mm^2 and a thickness h_f of 1.91 mm. Using the curved edges of the ferrite tile marked by the dashed line in Figure 3b, the desired hole for the via pin on the ferrite layer can be achieved easily without any additional process.

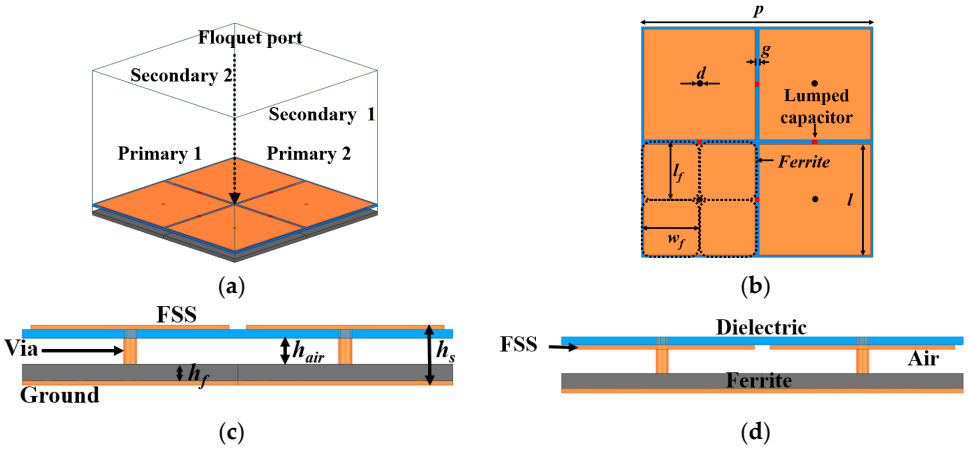


Figure 3. Unit cell simulation of the proposed design. (**a**) Simulation setup. (**b**) Top view. (**c**) Side view of the SML type. (**d**) Side view of the IML type.

An SML is a type of microstrip line (MSL) consisting of a thin metal strip suspended above a ground plane by a dielectric layer or spacers (air gap) and is designed for performance comparison with the proposed IML type in this work. An IML is a type of SML in which the suspended thin metal strip faces toward the ground plane. These types of MSLs are popular for millimeter- and micro-wave applications owing to their minimum attenuation, small effective dielectric constant, and low propagation and insertion losses. In addition, they provide less stringent dimensional tolerances and dispersion compared with conventional MSLs [30,31]. The lower losses in these types of MSLs are due to the air gap between the substrate and the ground plane, reducing the line dispersion. The IML design could be advantageous because it enables the utilization of the other side of the dielectric layer of the AMC, where the FSS patch is not printed. In other words, the metallic pattern of the Tx coil might be printed directly on top of the dielectric, which would minimize the overall weight and fabrication cost in a thinner profile. The infinite array of the unit cell simulation was performed using the high-frequency structure simulation (HFSS) tool from Ansys. The simulation setup and parameters can be found in Figure 3a,b.

As seen in Figure 3a, the unit cell boundaries are set for the vertical sides, and the top side is excited with the Floquet port to replicate plane wave excitation. In Figure 3b,

l is the length of the patch, g is the gap between each metal patch, and d is the diameter of the via pin. In Figure 3c, the total thickness of the AMC is h_s, and the gap between the ground and dielectric substrate is h_{air}. The values of the design parameter are l = 50.84 mm, g = 2 mm, d = 1.6 mm, h_s = 6.6 mm, and h_{air} = 3 mm. The thickness of the metal patch is 35 µm. We loaded lumped capacitors of 0.43 nF between the patches for miniaturization. The design of the SML and IML is mainly focused on achieving the zero-reflection phase at the target frequency of 6.78 MHz. The dimension of the unit cell including the size of the FSS is fixed considering the physical volume of the capacitors used in the design. Therefore, the performance optimization is carried out mainly based on h_{air}. This gap is tuned finely using parametric studies such that both array SML- and IML-based unit cells can operate at the target frequency. The simulated reflection phases of the two unit cells using SML and IML are plotted in Figure 4. In both cases, the lumped capacitance and other parameter values were kept the same. Figure 4 shows that the target frequency can be achieved in both cases owing to the additional inductance from the via pin and loaded ferrite cores.

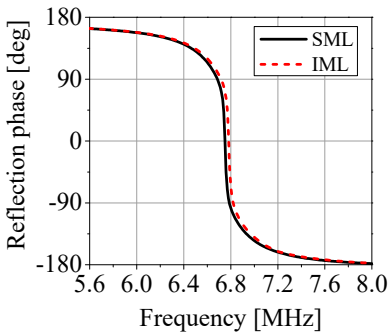


Figure 4. Reflection phase of the ferrite-loaded AMC unit cell.

3. WPTS Performance Simulation with AMC

3.1. WPTS without AMC

Tx and Rx coils were designed on the FR4 substrate with dimensions of 150 × 150 × 1.6 mm^3, as shown in Figure 5a, where the Tx and Rx coil coupling simulation setup without the AMC is given. The dielectric constant ε_r of the substrate is 4.4, and the loss tangent $tan\delta$ is 0.02. The width (t) and spacing (s) between the patterns are 2 and 3 mm, respectively. The number of turns is 7. A 59 pF lumped capacitor was used for resonance of approximately 6.78 MHz. To compare the WPTS performance according to the presence of the proposed AMC shielding, only the ferrite was placed behind the Tx coil, as shown in Figure 5b. Its dimension is 528 × 528 × 1.91 mm^3, as is that used in the AMC design in the next subsection. The Tx coil is positioned 4.5 mm from the ferrite tile. Figure 5c shows that the magnetic field is uniformly distributed in both the target and non-target regions for the WPTS simulation when no backing was used for the Tx coil. When only the ferrite tile was placed, the magnetic field was slightly reduced and not completely eliminated. The PTE performance was verified by varying the distance (d) between the Tx and Rx coils for both cases by measuring the PTE, defined by $|S_{21}|^2$, between the coils, as shown in Figure 5d. In Figure 5a, the PTEs of the WPTS at the distances of 10, 15, 20, and 30 cm are 64%, 17.64%, 4.84%, and 0.49%, respectively. The PTEs for the ferrite-only case at the distances of 10, 15, 20, and 30 cm are 20.25%, 2.89%, 1%, and 0.09%, respectively. Owing to ferrite loss, the PTE for the WPTS backed with a ferrite tile worsened by almost half compared with the case presented in Figure 5a.

3.2. WPTS with an AMC

The unit cell simulation shown in Figure 4 represents the infinite periodic array. For the finite array of the AMC surface, in this simulation, a 5-by-5 array of the AMC was used. Considering the unit cell size of 105.6 × 105.6 × 6.6 mm^3 for a 5 × 5 array, the total size of the AMC is 528 × 528 × 6.6 mm^3. The simulation setups of the SML- and IML-based

AMCs are shown in Figure 6a,b, respectively. For both cases, the AMC was placed 4.5 mm behind the Tx coil, as shown in Figure 6c. The magnetic shielding performance is presented in Figure 6d. The magnetic field at the backside of the Tx coil was eliminated after the placement of the SML- and IML-based AMCs. Small leakages at the edges due to the edge effect were observed. For the PTE performance shown in Figure 6e, the PTE is almost the same or slightly higher than the Tx–Rx coil simulations in Figure 5a without any back plate. For the SML type, the PTE values at the distances of 10, 15, 20, and 30 cm were 56.25%, 18.49%, 4.84%, and 0.64%, respectively, showing slightly degraded values compared with those of the case presented in Figure 5a, when no backing was used for the Tx coil. For the IML type, the PTE values at the distances of 10, 15, 20, and 30 cm were 68.89%, 24.01%, 6.76%, and 1.69%, respectively. In contrast to the case of SML-based AMC, the IML-based AMC showed improved PTE compared with the results presented in Figure 5a. This is due to the reduced dielectric losses of the IML design, in which the signal conductor of the FSS layer faces toward the ground plane, not toward the Tx coil, which can provide better control over the electric field distribution, resulting in lower dielectric loss than that with the conventional MSLs. Furthermore, the fields can be confined more between the FSS layer and the AMC ground plane to minimize radiation losses and improve the PTE.

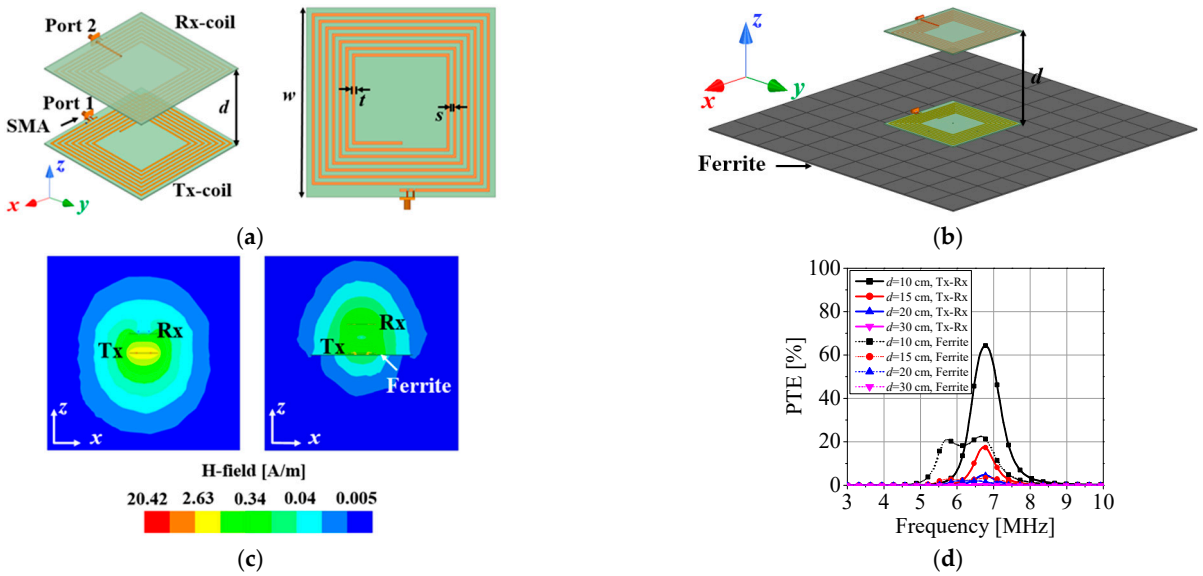


Figure 5. Tx–Rx coils only. (**a**) Simulation setup and parameters. (**b**) Simulation setup of the ferrite only as a shielding structure. (**c**) Magnetic field distribution. (**d**) PTE.

This study confirms the advantages of using the proposed AMC design in the WPTS. Among the three types of shielding structures, the IML-based AMC showed the best PTE performance. The shielding performance was almost the same for the two types of AMC. Owing to the lower IML loss than the usual MSL loss, the IML-based AMC did not retain high losses that could affect power transmission.

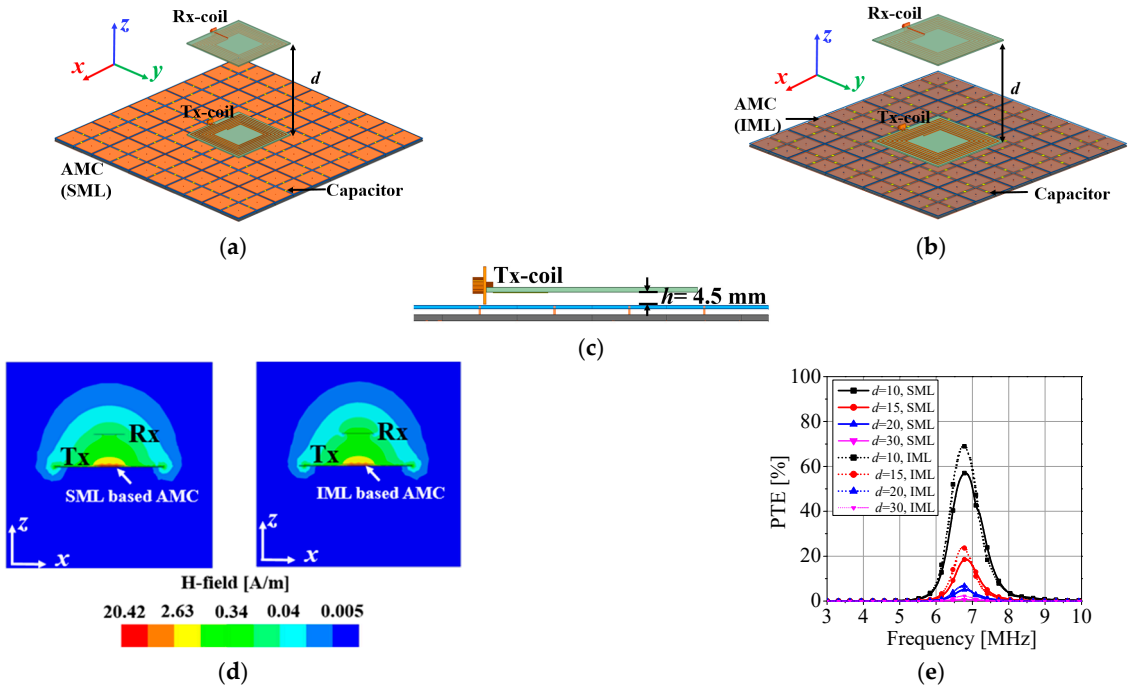


Figure 6. WPTS with the proposed AMC. (**a**) Simulation setup of SML-based AMC. (**b**) Simulation setup of IML-based AMC. (**c**) Simulation setup: side view. (**d**) Magnetic field distribution. (**e**) PTE.

4. Fabrication and Measurement

To verify the computed expectations from the full-wave EM simulations, the Tx coil, Rx coil, and AMC prototypes were built. The scattering parameters (S-parameters) and magnetic fields were measured to verify the performance of the WPTS with and without AMCs.

4.1. PTE Performance Verification

The built Tx and Rx coils are shown in Figure 7a. An SMA connector was soldered at each end of the coil, and a 56 pF lumped capacitor was loaded, creating resonance at 6.78 MHz. The coils were separated by Styrofoam of height d values of 10, 15, and 20 cm. The S-parameter was measured using a 2-port Anritsu MS42566B vector network analyzer (VNA). Figure 7b shows the measured PTE, calculated as $|S_{21}|^2 \times 100$ (%). The measured results showed a slight frequency shift of 2.95% compared with the simulation, possibly due to the fabrication tolerance and ground effect. Nevertheless, the Tx–Rx coil pair showed acceptable values for verifying the AMC performance. The measured peak PTE values shown in Figure 7b at the distances of 10, 15, 20, and 30 cm are 56.4%, 24.23%, 8.1%, and 2.04%, respectively.

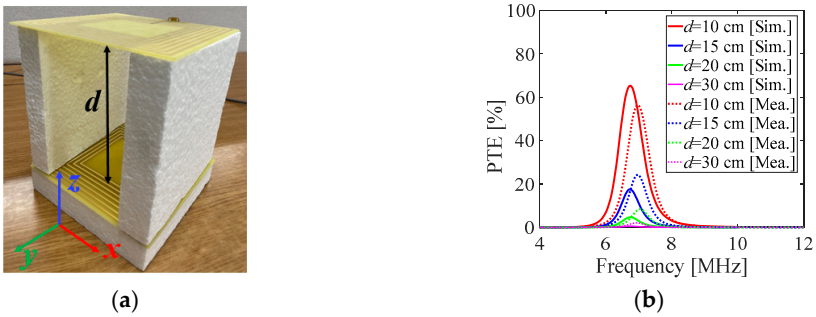


Figure 7. Fabrication and measurement. (**a**) Fabricated Tx–Rx coil prototype. (**b**) PTE.

For the AMC fabrication, the 5 × 5 array of the AMC surface was built. A quarter of the entire surface was built individually and then assembled. Two and a half unit cells

were present in the quarter of the 5 × 5 array of the AMC surface. The FSS patches of the unit cell in the quarter surface were connected by 0.43 nF capacitors, as in the simulation. Consequently, each quarter surface was connected by the 0.43 nF capacitors, again, as in the simulation, such that the 5 × 5 array of the AMC surface was assembled. This assembly procedure is illustrated in Figure 8. For better visualization, only the fabrication of a single unit cell composed of four FSS patches is shown in the figure. As shown in Figure 8a, the ground plane was prepared using a 528 × 528 mm^2 copper sheet and attached to the polystyrene foam board. Next, the ferrites were placed on top of the ground plane. The points of the via pin were marked, as illustrated in Figure 8b. After removing the ferrites, via pins were soldered at the marked points, as shown in Figure 8c. Then, the ferrites were properly arranged with the via pins, as in Figure 8d. Once everything was properly fixed, the printed FSS layer on the FR-4 substrate was reversed and placed on the top of the ferrite, as shown in Figure 8e,f. The gap between the ferrite and the printed FSS layer was achieved using small pieces of Styrofoam. In addition, the via pins were soldered to the dielectric substrate-based FSS layer, as marked by the red circles in Figure 8e. The side view of the built IML-based layers is shown in Figure 8f. The lumped capacitors faced toward the ground plane in the case of the IML-based AMC. Then, the Tx coil was placed on top of the AMC at a distance of 4.5 mm for the PTE and magnetic field leakage measurement.

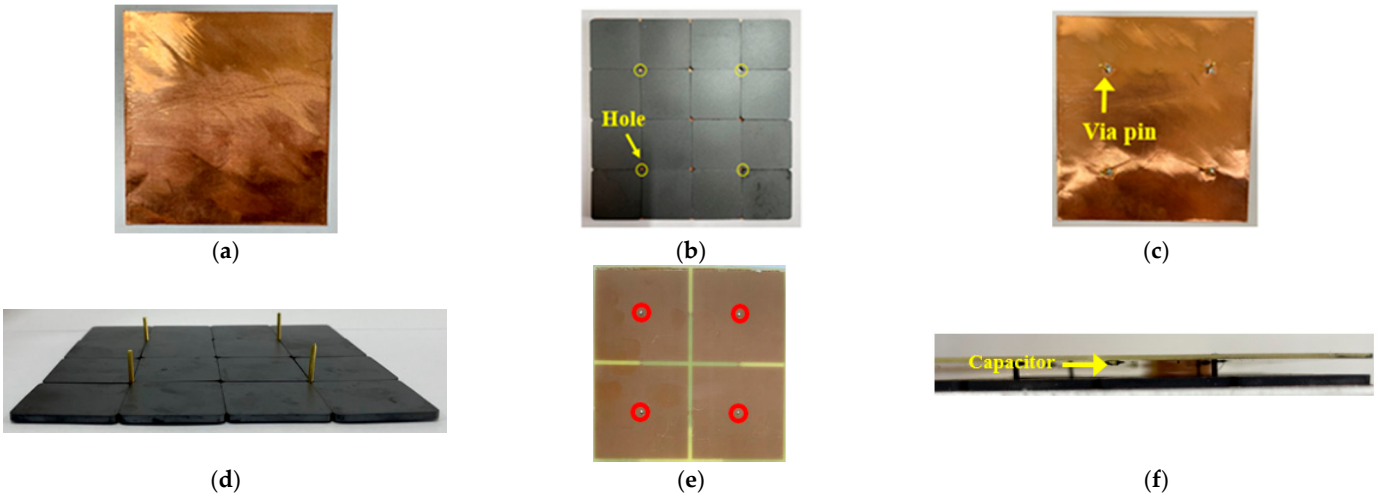
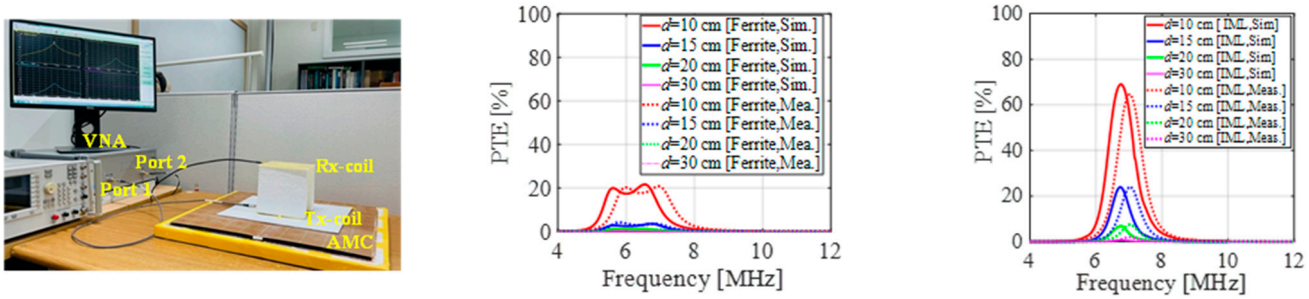


Figure 8. Procedure for assembling the AMC unit cell layers. (**a**) Ground plane. (**b**) Arrangement of ferrite and marking of the position of the hole. (**c**) Soldering the via pin on the ground plane using the marked position. (**d**) Rearrangement of ferrite on the via pin-connected ground plane. (**e**) Top view of the IML-based AMC. (**f**) Side view of the IML-based AMC.

Considering the PTE enhancement from the simulations, the PTE measurement was performed for the proposed IML-based AMC, as shown in Figure 9a. For the PTE measurements, the Tx and Rx coils were connected to ports 1 and 2 of the VNA, and the transfer coefficient S_{21} was measured by varying the distance (d) between the coils. The measured PTE values when the IML-type AMC was placed behind the Tx coil and in the case where only ferrite was placed behind the Tx coil are plotted in Figure 9b,c, respectively. The measured results were generally in good agreement with the simulations, showing the same trends observed in the simulations. The improved PTE values from the IML-based AMC-backed Tx–Rx coil pairs compared with the Tx–Rx coil pair in free space were verified, as it shows measured peak PTE values of 64.45%, 24.1%, 7.48%, and 1.95% at the distances of 10, 15, 20, and 30 cm, respectively.

The simulated and measured performance comparisons of the maximum PTEs are listed in Table 1. Overall, the WPTS with the proposed IML-based AMC design can provide a better power transmission characteristic than the WPTS without AMCs and with the ferrite-only-based magnetic shielding, in both the simulations and measurements. For the ferrite-only case, the PTE was almost half that in the case without shielding. For the

measured results of the IML case, the efficiency was slightly lower than the simulation results. The difference between the simulation and measurements could be due to the frequency shift of the Tx coil and AMCs and the losses from the core and additional lumped capacitors. Although the possible losses could degrade the PTE performance of the proposed AMC design in a real-time experimental environment, the PTE value was still higher than that in the case of the ferrite-only-based magnetic shielding structure.



(**a**) (**b**) (**c**)

Figure 9. Measurement results of the PTE. (**a**) Measurement setup. (**b**) Tx with ferrite only. (**c**) Tx with the IML-based AMC.

Table 1. PTE performance comparison of the proposed AMC design with the WPTS.

d	Simulated Maximum PTE at 6.78 MHz				Measured Maximum PTE at 6.98 MHz		
	without AMC		with AMC		without AMC		with AMC
	Tx–Rx Only	Ferrite Only	SML	IML	Tx–Rx Only	Ferrite Only	IML
10	64	20.25	56.25	68.89	56.4	20.7	64.45
15	17.64	2.89	18.49	24.01	24.23	3.42	24.1
20	4.84	1	4.84	6.76	8.1	0.87	7.48
30	0.49	0.09	0.64	1.69	2.04	0.14	1.95

4.2. Magnetic Shielding Performance Verification

To verify the magnetic shielding performance of the proposed AMCs, magnetic field leakage measurements were performed. The measurement setup is shown in Figure 10a. The Tx coil was fed with +20 dBm input power from an Anritsu MG3692C signal generator at a frequency of 6.98 MHz. A Keysight RF R 50-1 near-field probe was connected to an Anritsu MS2830A signal analyzer for the near-field scanning. The near-field probe has a better resolution of up to 10 cm. Therefore, the magnetic leakage measurement was performed along the $\pm z$-axis, as shown in Figure 10b, for distances up to 10 cm. The two cases of shielding structure, the IML- and ferrite-only-based AMCs, are shown in Figure 10c,d, respectively.

As shown in Figure 11a, the Tx–Rx coil pair in free space shows a uniform magnetic field distribution in both the target and non-target regions. The WPTS with IML-based AMC in Figure 11b clearly shows a high decrease in magnetic field, as in the simulations. In the ferrite-only case presented in Figure 11c, the magnetic field leakage was less than the case without a magnetic shielding structure but was not completely reduced, just as expected from the simulations. Overall, the measured field distribution was in good agreement with that of the simulation.

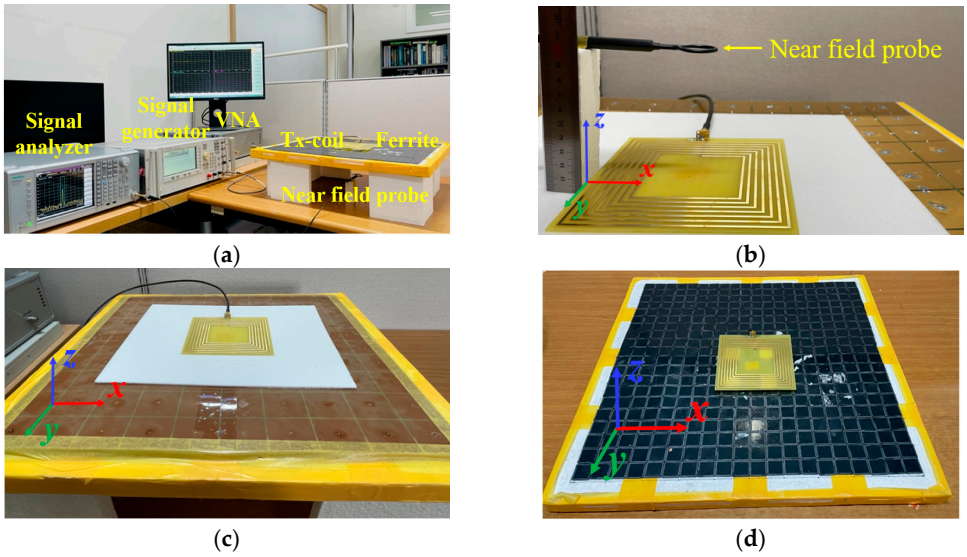


Figure 10. Measurement of magnetic shielding. (**a**) Measurement setup. (**b**) Near-field probe position. (**c**) IML-based AMC. (**d**) Ferrite only.

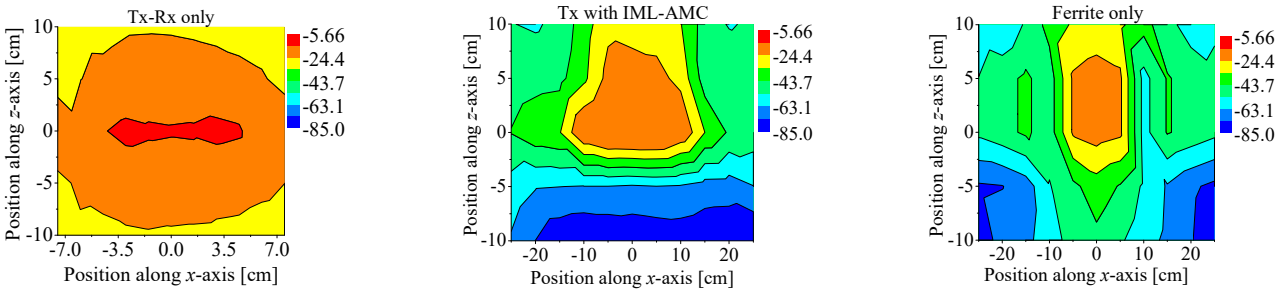


Figure 11. Measurement results of the magnetic field in dB scale. (**a**) Tx–Rx only. (**b**) Tx with the IML-based AMC. (**c**) Ferrite only.

Lastly, Table 2 shows the performance comparison between the proposed design and the previous work on AMC shielding for WPTS. The proposed IML-based AMC can improve the PTE by approximately 8% at 10 cm with an electrically small volume. It is also electrically thinner than other works reported in the literature. The dielectric-only substrate-based AMC operating at 26.5 MHz has a low profile but slightly larger electrical volume than its operating frequency. It caused a minimal improvement in PTE, approximately 3% at 6 cm and 16% at 1 cm, respectively [26]. Compared with the ferrite-based AMC work in [27], our proposed design offers better efficiency and lighter weight owing to the thinner ferrite profile used at approximately the same AMC surface area. It also shows a lower profile, including the gap between the Tx coil and the AMC.

The results based on the ideal PMC in the WPTS suggest a magnetic field improvement of approximately 50% [25]. However, the ferrite and resistive losses from the capacitors affected the PTE. Nevertheless, the proposed AMC still achieved complete magnetic shielding and showed improved PTE at certain distances. This research highlights the suitability of using AMC at a 6.78 MHz WPTS without compromising the PTE performance. In the future, the development of high-permeability materials for high-frequency applications could further improve the PTE and enable the design of a more compact AMC.

Table 2. Measured performance of the proposed design compared with those in previously published works.

Reference	Design Concept	Frequency (MHz)	Physical Size (mm^3)	Electrical Volume (λ^3)	Measured PTE Improvement (%)	Shielding Effect
[26]	Dielectric substrate only	26.2	$348 \times 348 \times 5$ Less weight and easier and inexpensive fabrication	$0.0304 \times 0.0304 \times 0.00044$	16 at 1 cm 3 at 6 cm (Measurement)	Good
[27]	Ferrite substrate	6.78	$520 \times 520 \times 5$ Possibly heavy and expensive fabrication (via the ferrites)	$0.0117 \times 0.0117 \times 0.00011$	NA *	NA *
This work	Dielectric and ferrite substrate	6.98	$528 \times 528 \times 6.6$ Less weight and inexpensive fabrication	$0.0122 \times 0.0122 \times 0.00014$	8.05 at 10 cm (Measurement)	Good

* NA—Not applicable.

5. Conclusions

In this study, to overcome the limitation of the dielectric-based AMC for low frequencies, possible design methods were studied and proposed. The proposed design performance was analyzed and verified for WPTS applications. The performance of the proposed IML-based AMC design has been verified experimentally. To the best our knowledge, this is the first work on AMC design that shows the measurement results for a target frequency of 6.98 MHz. The proposed design showed very good magnetic shielding performance and slightly improved PTE performance. In addition, it showed better PTE and magnetic shielding performances than the ferrite-only-based AMC. Therefore, the proposed IML-based AMC design could be a solution to the magnetic leakage problem while maintaining or improving PTE performance. To achieve the best PTE improvement, the losses could be minimized by selecting the ferrite material, which has high permeability with minimum loss.

Author Contributions: Conceptualization, S.M.R. and I.-J.Y.; methodology, S.M.R., J.H.L. and I.-J.Y.; software, S.M.R., J.H.L. and I.-J.Y.; validation, S.M.R., S.H.C., I.-K.C. and I.-J.Y.; formal analysis, S.M.R., J.H.L., J.H.O., I.-K.C. and I.-J.Y.; investigation, S.M.R., S.H.C., J.H.O. and I.-J.Y.; resources, S.M.R., J.H.L., J.H.O., I.-K.C. and I.-J.Y.; data curation, S.M.R., S.H.C., J.H.O., I.-K.C. and I.-J.Y.; writing—original draft preparation, S.M.R.; writing—review and editing, I.-J.Y.; visualization, S.M.R.; supervision, I.-J.Y. All authors have read and agreed to the published version of the manuscript.

Funding: This work was funded in part by the Electronics and Telecommunications Research Institute under Grant No. 23ZH1140 and in part by the Institute of Information and Communications Technology Planning and Evaluation (IITP) grant funded by the Korea government (MSIT; No. 2020-0-00839, Development of Advanced Power and Signal EMC Technologies for Hyper-connected E-Vehicles).

Conflicts of Interest: The authors declare no conflict of interest.

References

1. Tseng, R.; von Novak, B.; Shevde, S.; Grajski, K.A. Introduction to the alliance for wireless power loosely-coupled wireless power transfer system specification version 1.0. In Proceedings of the 2013 IEEE Wireless Power Transfer (WPT), Perugia, Italy, 15–16 May 2013; pp. 79–83.
2. Yoon, I.-J.; Ling, H. Realizing efficient wireless power transfer using small folded cylindrical helix dipoles. *IEEE Antennas Wirel. Propag. Lett.* **2010**, *9*, 846–849. [CrossRef]
3. Garnica, J.; Chinga, R.A.; Lin, J. Wireless power transmission: From far field to near field. *Proc. IEEE* **2013**, *101*, 1321–1331. [CrossRef]
4. Ali, A.; Ehsan, A.S.; Seyedreza, A.; Patrick, W. Analytical modeling of self- and mutual inductances of DD coils in wireless power transfer applications. *J. Electromagn. Eng. Sci.* **2022**, *22*, 162–170.

5. Costanzo, A.; Masotti, D. Energizing 5G: Near- and far-field wireless energy and data transfer as an enabling technology for the 5G IoT. *IEEE Microw. Mag.* **2017**, *18*, 125–136. [CrossRef]
6. Hui, S.Y.R.; Zhong, W.; Lee, C.K. A Critical review of recent progress in mid-range wireless power transfer. *IEEE Trans. Power Electron.* **2014**, *29*, 4500–4511. [CrossRef]
7. Leyh, G.E.; Kennan, M.D. Efficient wireless transmission of power using resonators with coupled electric fields. In Proceedings of the 2008 40th North American Power Symposium, Calgary, AB, Canada, 28–30 September 2008.
8. Kurs, A.; Moffatt, R.; Soljačić, M. Simultaneous mid-range power transfer to multiple devices. *Appl. Phys. Lett.* **2010**, *96*, 044102. [CrossRef]
9. International Commission on Non-Ionizing Radiation Protection (ICNIRP). Guidelines for limiting exposure to electromagnetic fields (100 kHz to 300 GHz). *Health Phys.* **2020**, *118*, 483–524. [CrossRef]
10. Mizuno, T.; Yachi, S.; Kamiya, A.; Yamamoto, D. Improvement in efficiency of wireless power transfer of magnetic resonant coupling using magneto plated wire. *IEEE Trans. Magn.* **2011**, *47*, 4445–4448. [CrossRef]
11. Zhang, X.; Ho, S.L.; Fu, W.N. Quantitative design and analysis of relay resonators in wireless power transfer system. *IEEE Trans. Magn.* **2012**, *48*, 4026–4029. [CrossRef]
12. Tang, S.; Hui, S.; Chung, H.-H. Evaluation of the shielding effects on printed-circuit-board transformers using ferrite plates and copper sheets. *IEEE Trans. Power Electron.* **2002**, *17*, 1080–1088. [CrossRef]
13. Zhang, X.; Han, R.; Li, F.; Pan, X.; Chu, Z. Design and analysis of magnetic shielding mechanism for wireless power transfer system based on composite materials. *Electronics* **2022**, *11*, 2187. [CrossRef]
14. Ahn, J.; Kim, J.; Park, D.; Kim, H.; Ahn, S. An active shielding control method for a wireless power transfer system under misalignment conditions. *J. Electromagn. Eng. Sci.* **2022**, *22*, 56–63. [CrossRef]
15. Park, J.; Kim, D.; Hwang, K.; Park, H.H.; Kwak, S.I.; Kwon, J.H.; Ahn, S. A Resonant reactive shielding for planar wireless power transfer system in smartphone application. *IEEE Trans. Electromagn. Compat.* **2017**, *59*, 695–703. [CrossRef]
16. Mohammad, M.; Wodajo, E.T.; Choi, S.; Elbuluk, M.E. Modeling and design of passive shield to limit emf emission and to minimize shield loss in unipolar wireless charging system for EV. *IEEE Trans. Power Electron.* **2019**, *34*, 12235–12245. [CrossRef]
17. Lee, W.; Yoon, Y.-K. Wireless power transfer systems using metamaterials: A review. *IEEE Access* **2020**, *8*, 147930–147947. [CrossRef]
18. Cho, Y.; Lee, S.; Jeong, S.; Kim, H.; Song, C.; Yoon, K.; Song, J.; Kong, S.; Yun, Y.; Kim, J. Hybrid metamaterial with zero and negative permeability to enhance efficiency in wireless power transfer system. In Proceedings of the 2016 IEEE Wireless Power Transfer Conference (WPTC), Aveiro, Portugal, 5–6 May 2016; p. 13.
19. Ranaweera, A.; Duong, T.P.; Lee, J.-W. Experimental investigation of compact metamaterial for high efficiency mid-range wireless power transfer applications. *J. Appl. Phys.* **2014**, *116*, 043914. [CrossRef]
20. Sievenpiper, D.; Zhang, L.; Broas, R.; Alexopolous, N.; Yablonovitch, E. High-impedance electromagnetic surfaces with a forbidden frequency band. *IEEE Trans. Microw. Theory Tech.* **1999**, *47*, 2059–2074. [CrossRef]
21. Clavijo, S.; Diaz, R.E.; McKinzie, W.E. Design methodology for Sievenpiper high-impedance surfaces: An artificial magnetic conductor for positive gain electrically small antennas. *IEEE Trans. Antennas Propag.* **2003**, *51*, 2678–2690. [CrossRef]
22. Feresidis, A.P.; Goussetis, G.; Wang, S.; Vardaxoglou, J.C. Artificial magnetic conductor surfaces and their application to low-profile high-gain planar antennas. *IEEE Trans. Antennas Propag.* **2005**, *53*, 209–215. [CrossRef]
23. Ta, S.X.; Park, I. Design of miniaturized dual-band artificial magnetic conductor with easy control of second/first resonant frequency ratio. *J. Electromagn. Eng. Sci.* **2013**, *13*, 104–112. [CrossRef]
24. Shin, G.; Park, T.R.; Park, J.; Lee, S.-K.; Kim, G.; Yoon, I.-J. Sustaining the radiation properties of a 900-mhz-band planar lora antenna using a 2-by-2 thin ebg ground plane. *IEEE Access* **2020**, *8*, 145586–145592. [CrossRef]
25. Wu, J.; Wang, B.; Yerazunis, W.S.; Teo, K.H. Wireless power transfer with artificial magnetic conductors. In Proceedings of the 2013 IEEE Wireless Power Transfer (WPT), Perugia, Italy, 15–16 May 2013; pp. 155–158.
26. Shi, T.; Dong, L.; Chen, Y.; Sun, Y.; Liu, Y.; Deng, F.; Liu, L.; Shi, Y.; Shen, Y. Using artificial magnetic conductors to improve the efficiency of wireless power transfer. *AIP Adv.* **2019**, *9*, 045308. [CrossRef]
27. Lawson, J.; Yates, D.C.; Mitcheson, P.D. Efficient artificial magnetic conductor shield for wireless power. In Proceedings of the 2015 IEEE Wireless Power Transfer Conference, Boulder, CO, USA, 13–15 May 2015; pp. 1–4.
28. MP1040-200. Available online: https://media.digikey.com/pdf/Data%20Sheets/Steward%20PDFs/Ferrite_EMI_Disks_Plates.pdf (accessed on 21 April 2022).
29. Rafaei-Booket, M.; Atlasbaf, Z.; Shahabadi, M. Metallic grating on a periodic anisotropic substrate as a planar artificial magnetic conductor. In Proceedings of the 2016 8th International Symposium on Telecommunications (IST), Tehran, Iran, 27–28 September 2016; pp. 419–423.
30. Musa, S.M.; Sadiku, M.N.O. Modeling of shielded, suspended and inverted, microstrip lines. In Proceedings of the IEEE SoutheastCon 2008, Huntsville, AL, USA, 3–6 April 2008; pp. 309–313.
31. Yamina, B.; Nasreddine, B.; Nadia, B.; Kamila, A.; Fethi, B. Closed-form formulas for the electromagnetic parameters of inverted microstrip line. *Intl. J. Eng. Res. Dev.* **2012**, *1*, 2267–2278.

Disclaimer/Publisher's Note: The statements, opinions and data contained in all publications are solely those of the individual author(s) and contributor(s) and not of MDPI and/or the editor(s). MDPI and/or the editor(s) disclaim responsibility for any injury to people or property resulting from any ideas, methods, instructions or products referred to in the content.